HiSST: 3rd International Conference on
High-Speed Vehicle Science Technology
14 -19 April 2024, Busan, Korea

STORT Hypersonic Flight Experiment CMC Thermal Protection System and Selected Flight Results

T. Reimer[1], G. D. Di Martino[1], L. Dauth[2], L. Baier[1], A. Gülhan[3], F. Klingenberg[3], D. Hargarten[4]

[1]DLR Institute of Structures and Design, 70569 Stuttgart, Germany
[2]Bayern-Chemie GmbH, 84544 Aschau am Inn, Germany
[3]DLR Institute of Aerodynamics and Flow Technology, 51147 Cologne, Germany
[4]DLR Space Operations and Astronaut Training, 82234 Wessling, Germany

Abstract

The DLR project STORT was focused on investigating key key technologies for flight at hypersonic Mach numbers of higher than 8. The main goal of the project is to enable cost reduction of future space transportation systems while keeping them reliable. To this end, reusability of the stages of a launcher system is a necessity. For first stages, a Mach number of 8-10 seems to be the optimum staging velocity, which means that technologies for the return flight of first stages at those speeds need to be developed and validated. Consequently, STORT aimed at achieving such operating conditions at Mach 8, to support the optimization and validation of technologies and simulation tools for the development of future space transportation systems.
The present paper describes the design, manufacturing and integration of the rocket forebody assembly. The forebody thermal protection system structures require the use of ceramic matrix composite material for protection from the high heat loads experienced during the flight. In the present case the thermal protection system was constituted by C/C-SiC composite structures built in-house by DLR. The main elements were a conical nose element and four thin-walled shell segments manufactured via filament winding of carbon fibers fitted with integral fixation brackets. In addition, selected flight data collected on the thermal protection system is presented.

Keywords (Tahoma 10 pt, bold): *Ceramic Matrix Composites, Thermal Protection System, Hypersonic Flight Experiment*

Nomenclature (Tahoma 11 pt, bold)

C/C – Carbon/carbon
C/C-SiC – C/C reinforced silicon carbide
CFRP – Carbon fiber reinforced plastic
CMC – Ceramic Matrix Composite
DLR – German Aerospace Center
LSI – Liquid silicon infiltration
q – heat flux density
RMI – Reactive melt infiltration
STORT – Schlüsseltechnologien für hochenergetische Rückkehrflüge der Trägerstufen
TPS – Thermal protection system
h – heat transfer coefficient
T_r – Recovery temperature
T_w – Wall temperature

1. Introduction

Sounding rocket flight experiments are an important building block in the development and optimization of future space transportation systems, because they provide for a cost-efficient opportunity to collect valuable flight data in a real flight environment which is required, both for compensating the deficits of ground experimental testing and for providing the input data for the definition and validation of reliable numerical tools. With this objective, DLR has been working on a number of experimental flight test projects over recent years with the objective of demonstrating technologies for reusable first stage

launchers. While such previous and ongoing DLR projects focus on aerodynamics and control at Mach numbers lower than 5 [1,2,3] with correspondingly moderate heat loads, the focus of the STORT project was on the thermomechanical challenges encountered by thermally highly loaded components at high Mach numbers (at or higher than 8) for a relatively long time, of approximately 2 minutes [4]. As a result, high heat loads were encountered for such a relatively long time, thus obtaining more representative conditions of high-energetic re-entry flights for application in reusable first or even upper stages. In this framework, the DLR Institute of Structures and Design was responsible for the design, manufacture, assembly and testing of the forebody of the sounding rocket for the flight experiment. The CMC external structures were subjected to high heat loads and mechanical loads during the flight, therefore they needed to be made of ceramic matrix composite (CMC) materials and the design process had to consider a challenging thermo-mechanical environment.

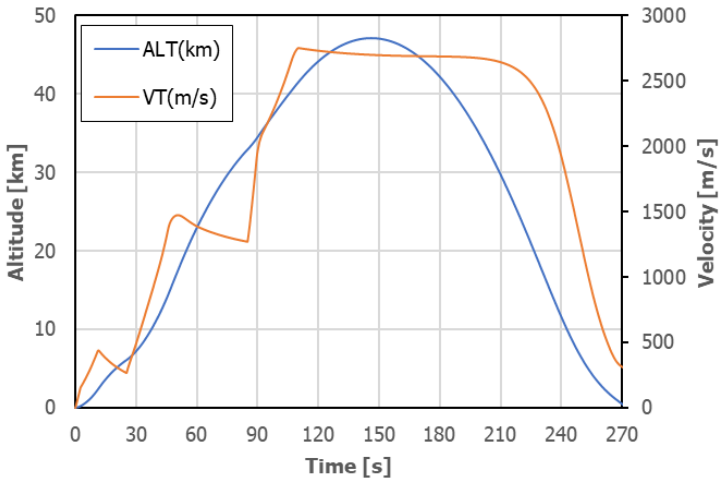

Fig. 1. STORT flight experiment nominal trajectory.

In Fig. 1 the STORT flight experiment nominal trajectory is shown. In the velocity graph the phases of the three-stage flight can be recognized, and in Table 1 the main events of the flight are listed.

Table 1. Main events during the STORT flight.

Event	Time [s]	Altitude [km]
S31 Motor Ignition	0	0.04
S31 Motor Separation (passive)	11.5	2.48
S30 Motor Ignition	24	5.84
S30 Motor Burnout	51.1	18.7
S30 Motor Separation (active)	60	23.87
IO Motor Ignition	88	34.69
IO Motor Burnout	113	42.08
Apogee	141,9	45.73
Impact	265.4	-0.02

2. Structure Concept

The overall structure concept foresees a metallic load-bearing structure within the payload forebody on which a thermal protection system (TPS) aeroshell is installed that transfers aerodynamic loads to the metallic structure via dedicated attachment points. In Fig. 2 a cross section of the forebody structure with the TPS structures is shown. The space between metallic and TPS structure was filled with a flexible high-temperature insulation.

One main requirement in the design process was to obtain a smooth external surface, which would allow to investigate the aerodynamic phenomena typical of the hypersonic flow. As a result, the forebody TPS should consist of a number of structures as low as possible to reduce the number of parts and thus interfaces on the external surface. The selected design comprised a bulk nose element and four axisymmetric shell segments. The TPS shell structures of the forebody consisted of a specifically designed and in-house manufactured ceramic matrix composite (CMC) structure which is a carbon fiber-reinforced ceramic, described as C/C-SiC. The material is produced via the Reactive Melt Infiltration (RMI) process, also referred to as the Liquid Silicon Infiltration (LSI) process, specifically for this material type. The matrix is a mix of amorphous carbon in the fiber bundle blocks surrounded by silicon carbide and small amounts of residual silicon.The shell structures were manufactured via wet filament winding of a carbon fiber with a polymeric resin and subsequent pyrolysis and liquid silicon infiltration.

The metallic structure inside of the forebody was an aluminium structure consisting of individual elements of frames, stringers and skins, all of which were assembled via screws.

In order to provide attachment points to the wound CMC shell structures, the in-situ joining method [5], was implemented to attach CMC brackets to the insides of the shell structures. Thus, the TPS could be connected to the metallic understructure while avoiding surface disturbances which would affect the external aerodynamic flow. In past projects, another system of TPS attachment had been used, based on the use of ceramic screws [SHEFEX]. This system has other advantages, e.g. that it can be mounted from the external surface without access to the structure below, but in this case the system of cold (warm) attachment with a combination of CMC/metallic components was used to avoid surface disturbances.

The selected design of the double-l connections provides for mechanical strength as well as for sufficient elasticity to compensate for thermal expansion differences between the hot CMC structures on the surface and the cold metallic structure inside of the forebody.

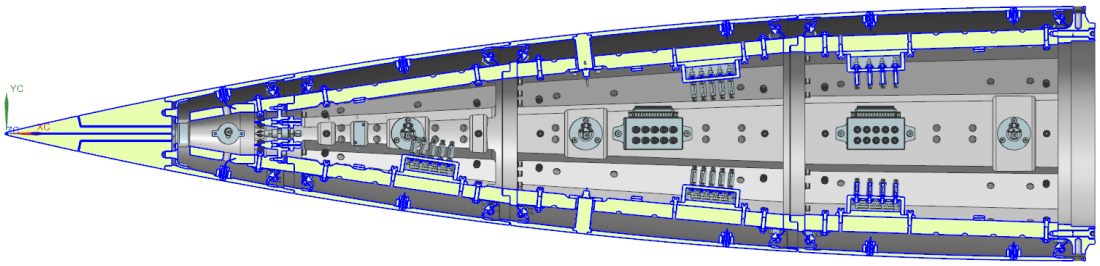

Fig. 2. STORT forebody overall cross section of structure and TPS.

The design of the double-l connection is critical to the function of the overall system. It was developed over several iterations with a number of possible designs to start with. Other design solutions that were looked at included fully ceramic connections to be joined to the inside of the ceramic shells. Finally, a design was chosen which uses a combination of ceramic angled brackets, joined via in-siut joining to the ceramic shells, and corresponding metallic brackets. Via numerical simulation the design was finalized with regard to the actual dimensions of the ceramic and metallic brackets. The advantages of the selected design are that the components are relatively easy to produce, position adjustments during assembly can be made to account for misalignemnts and stress control is good. The disadvantage is that the in-situ joining of each of the bracket components is a possible fault source during production which could have led to non-acceptance of the shell structure.

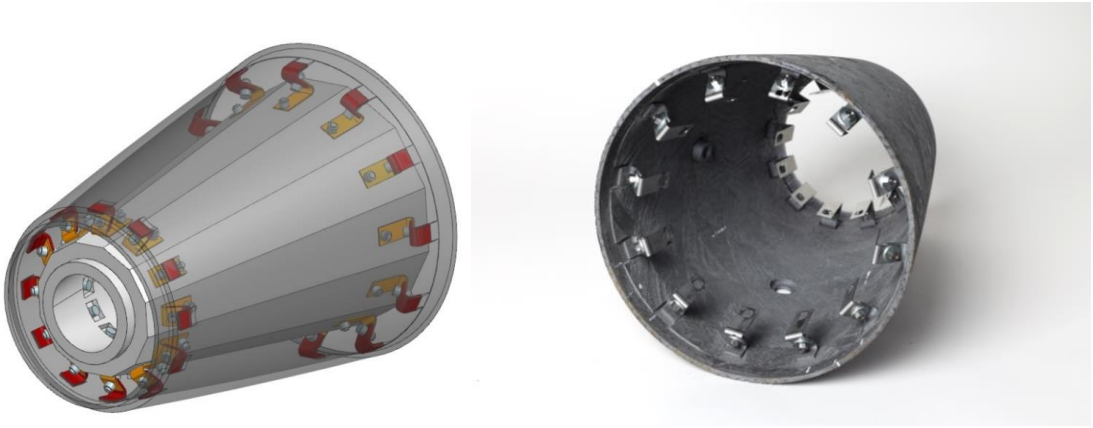

Fig. 3. CAD design of the double-l connection (left) and hardware image (right).

Fig. 4 shows a view of the assembled forebody with CMC TPS and the payload modules located behind the CMC forebody. Note that directly after the CMC forebody, there is the so-called fin module that featured three fixed CMC fins representing typical aerodynamic control surfaces to investigate internal active cooling technologies for such structures.

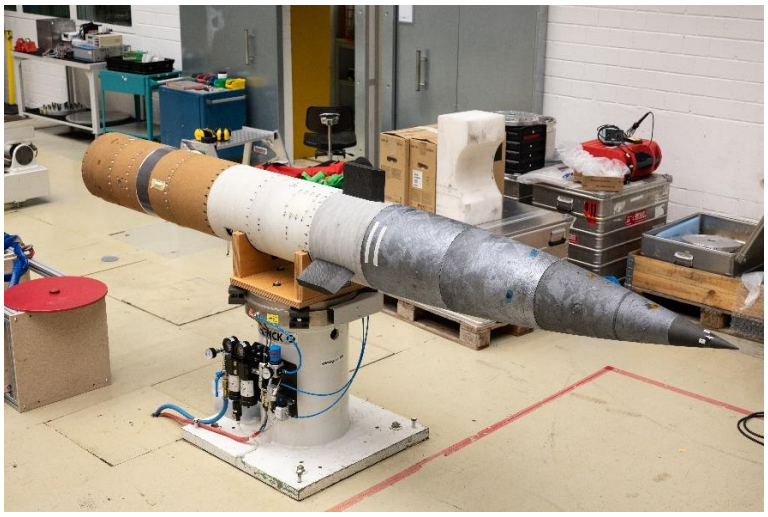

Fig. 4. STORT forebody and payload modules.

3. Thermo-mechanical structure validation

Numerical simulations were done to analyze the forebody structures in order to support the design process and validate the overall resistance of the structures.

First, an estimation of the thermal response of the CMC thermal protection system surface structures was obtained by an iterative procedure based on the general equation for the convective heat flux $\dot{q}_{conv}$, given by

$$\dot{q}_{conv} = h(T_r - T_w) \quad (1)$$

where the heat transfer coefficient h was estimated with literature correlation equations [6,7] using different formulations for the stagnation area and for the different segments. The recovery temperature T_r was estimated based on the trajectory data. The estimated heat flux was given as boundary condition, together with the radiation energy emission of the body to the external environment, for a

transient thermal simulation. Since the hot wall temperature is at first unknown, an iterative approach was performed, where the transient heat flux density was newly calculated after each iteration using the preceding result of the wall temperature. The hot wall temperature, and thus the hot wall heat flux, had converged after a few iterations. Fig. 5 shows the results in terms of convective heat flux and maximum wall temperature expected during the trajectory on the different segments of the TPS structure.

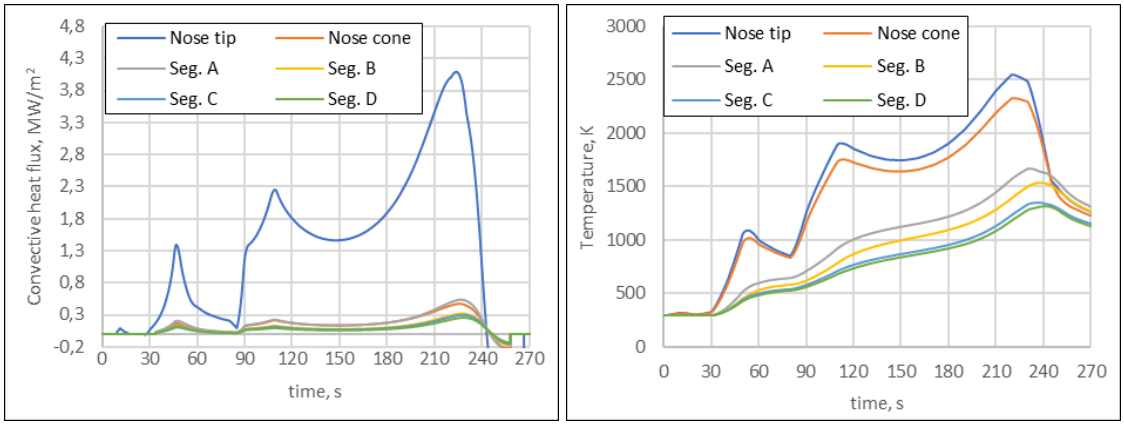

Fig. 5. Calculated convective heat flux and wall temperature on the TPS segments.

The calculated temperature distributions were then considered as load conditions for a static mechanical analysis to estimate the structure thermal expansion and the associated stresses. In Fig. 6 the calculated surface temperatures for the maximum temperature condition are depicted. Note that the temperture on segment A is higher than the rear part of the nose tip, due to the fact that the nose tip is a solid structure without internal empty space, whereas the following segments are thin walled structures. Other load cases for the structure validation included the expected most critical aerodynamic pressure load, axial and transversal acceleration loads and vibration load.

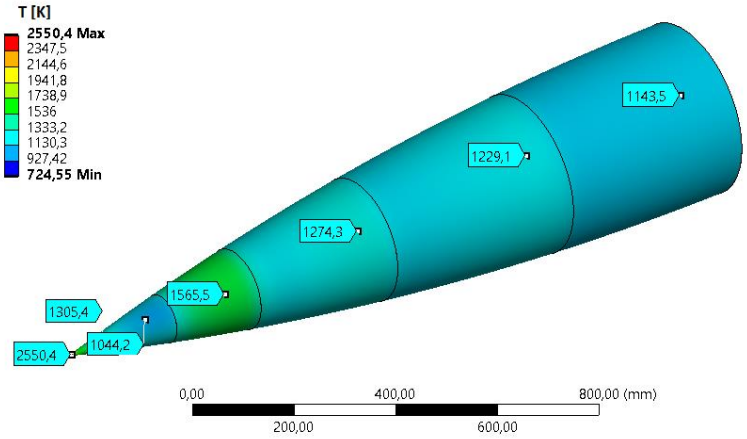

Fig. 6. Calculated temperature distribution on the TPS at t=230 s.

The double-I connection between the CMC shells and the metallic structure was the critical mechanical element of the forebody. The stress analysis of the CMC bracket and the Inconel bracket was done for the critical combination of loads, with regard to thermal load and pressure load. The most critical combination was observed at the flight time of 217 s which is at the second peak of the thermal load when the pressure is also constantly increasing. One example of a stress analyis of both brackets of segment B is shown in Fig. 7 with thermal load only at 230 s.

In this case the mechanical analysis for both brackets showed stresses of 103 MPa for the CMC element and 290 MPa for the Inconel part. A bending stress of 180 MPa for the CMC material was considered as the limit, for the Inconel 600 the limit acceptable stress was 550 MPa.
In the most severe load case combination with non-symmetric pressure load due to an angle of attach of 10°, the combined temperature-pressure load resulted in a stress of 171 MPa in the CMC bracket of segment D. For the Inconel brackets the stress was always much lower than the limit stress.

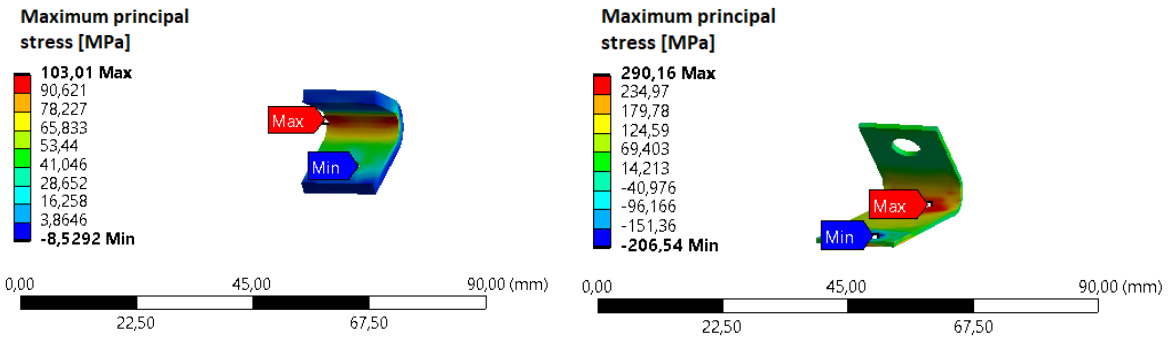

Fig. 7. Stress at t=230 s in the seg B CMC bracket (left) and in the Inconel bracket (right) as a result of only thermal load leading to thermal expansion.

4. Hardware manufacturing and assembly

The aluminium metallic structure was made by standard milling processes. Integral frames at the beginning and at the end of the respective segments were connected via one-piece milled stringer parts. Thin-walled sheets were placed in the openings of the assembled frame. Fig. 8 shows the arrangement of the individual components (left) and the assembled metallic structure (right).

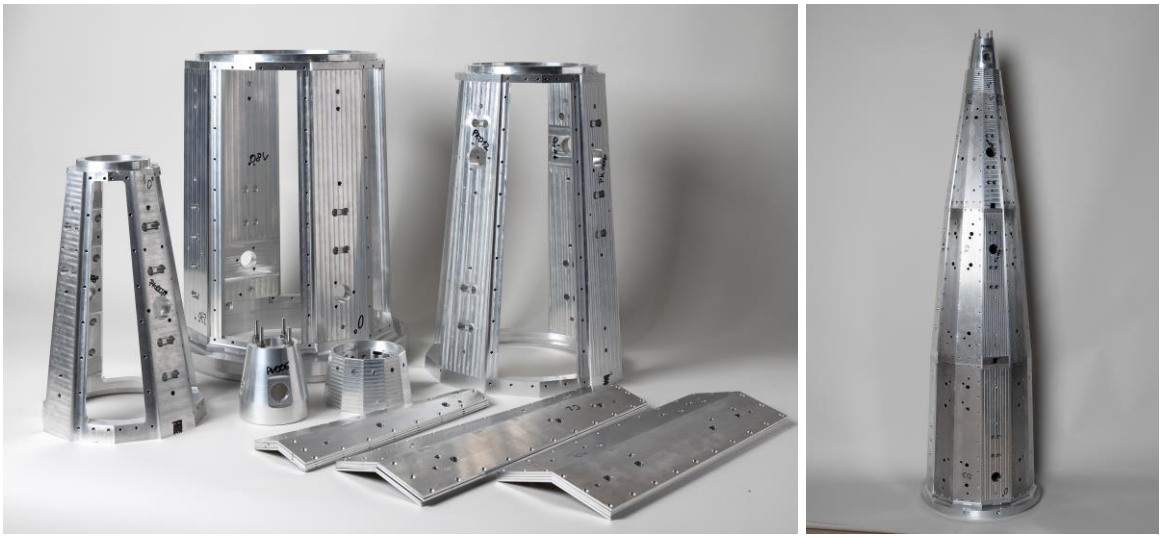

Fig. 8. Metallic structure components (left), assembled structure (right).

The CMC components of the forebody TPS were manufactured in-house at the Institute of Structures and Design of DLR in Stuttgart. As mentioned, the design was based on the use of axisymmetric shell segments, for which the manufacturing process consisted of the following steps

- Manufacturing of the green body CFRP part via wet filament winding
- Pyrolysis process to create an intermediate stage C/C component
- In-situ joining of the connection elements in C/C condition
- Reactive melt infiltration with liquid silicon to create the C/C-SiC final component

Fig. 3 shows a picture of two of the CMC segments in the final C/C-SiC condition. On the left hand side, the largest shell segment D is shown, on the right hand side, the smallest shell segment A is shown that is located directly after the bulk nose tip. Several boreholes are visible, which serve to accommodate sensor elements.

Fig. 9. C/C-SiC segments D (left) and A (right).

The first step in the assembly procedure was a fit check of the CMC Shell structures with its corresponding metallic sub-structure and the metallic connection brackets. When the relative position of the CMC shell and the metallic structure was acceptable, the connection elements were fixed in their final position and the bolts and nuts tightened and secured. Afterwards the shell was removed again from the metallic structure, with the metallic connection elements still attached to it to proceed to the step of sensor integration which is shown in Fig. 10 (left). The sensors installed were thermocouples, heat flux gauges and pressure sensors. The heat flux gauges were coaxial thermocouples. In the segments behind the nose, only type K thermocouples were installed, in the nose type B thermocouples were used. The pressure sensors were mounted in a dedicated CMC component that included also one coaxial thermocouple to have a pressure and heat flux reading in nearly the same position. This sub-assembly was the so-called combi-sensor.
After the installation of the sensors, the high temperature insulation was placed inside the ceramic shell structure, shown in Fig. 10 (right) and the metallic structure was placed inside. Due to the preceding fit check and the pre-assembled metallic connection brackets, the mounting of the metallic structure in the CMC shell (including sensors and insulation) proved to work well. In Fig. 11 (left) an image of the pre-assembled segment B is shown, ready for forebody mating.

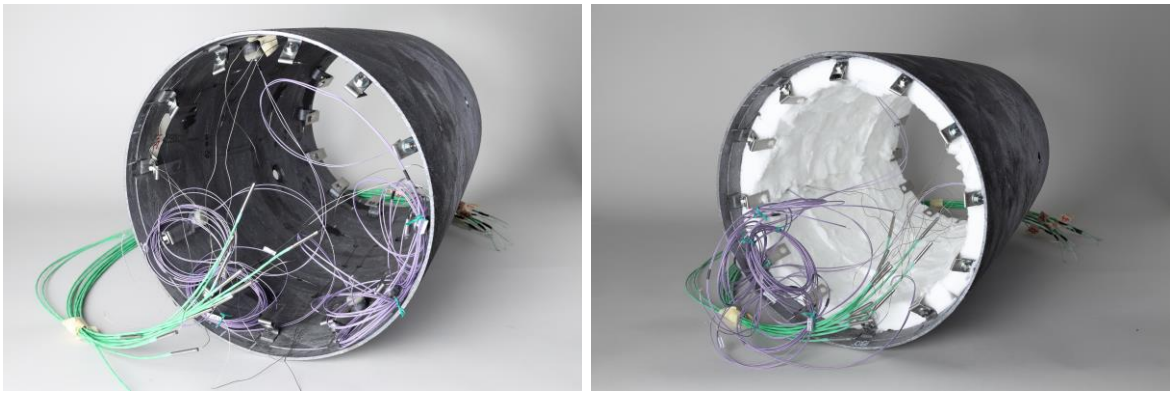

Fig. 10. CMC shell segment with installed sensors (left) and with installed high-temperature insulation (right).

The fully assembled segments were mated together vertically starting from the nose. The mechanical connection between two neighbouring segments was done via a bolt circle on the front and end frame

of each of the metallic substructures. While this process was carried out, the cable routing was done in parallel to feed the sensor cables from the front of the forebody to several break-out-boxes that were located inside of the metallic structure of the forebody.

Fig. 11. STORT segment B before assembly (left) and the STORT forebody fully assembled (right).

The main problems encountered during the assembly process were the cable routing from the pre-assembled heat flux sensors through the metallic structure while the metallic structure was inserted and fixed in the CMC shell structure. Especially in the case of segment D, which has an almost tubular shape, this proved to be problematic since the sensor size was almost as large as the space between CMC shell and metallic structure. Thus some cable damage was resulting and mandated repair. In addition, also the cable routing and connector placement to the break-out boxes during the mating of the forebody was quite challenging as there were so many sensors that needed to be routed and connected in the process. Furthermore, this had to be done in such a way as to make sure that the cables and connections can sustain the vibration load environment during launch. The assembled forebody as shown in Fig. 11 (right).

5. Flight Results

The flight of the STORT experimental vehicle was fully successful. The data of the sensors installed in the TPS could be transmitted to the ground station via telemetry until the vehicle was at a low altitude. The achieved trajectory was slightly more shallow than the planned one . The maximum altitude was 38 km instead of 45 km, thus resulting in higher heat loads than expected. The achieved Mach number was as planned for the first part of the flight with a maximum of Mach 8.25 at 106.4 s and just under Mach 8 up to 166.4 s when it started to decrease again. So for a duration of one minute the Mach number was quite constant around Mach 8. Table 2 gives the flight times when characteristic Mach numbers are passed on the ascent and on the descent and the corresponding duration of the flight between those numbers. When Mach 7.5 is considered, the flight time above is almost one minute and a half.

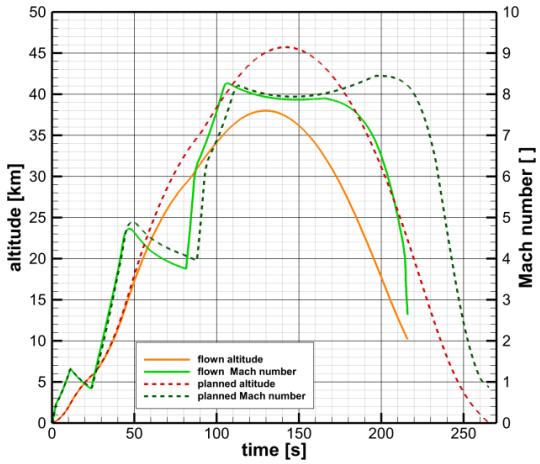

Fig. 12. STORT predicted and flown trajectory.

Table 2. Selected Mach number flight times on the ascent and on the descent.

Mach, -	Ascent time, s	Descent time, s	Duration, s
8	103.1	121.7	18.6
7.5	99.4	185.6	86.2
7	95.2	194.4	99.1
5	84.3	209.8	125.5

Fig. 13 shows a sketch of the temperature measurement positions over the forebody. There were four lines of temperature measurements over the forebody, starting from the stagnation point and distributed by 90° sectors over the circumference of the forebody. On the segments A – D the nominal measurement depth of the thermocouples was 2 mm below the surface. The tips of the thermocouples had been embedded in grooves within the CMC shell and covered with high temperaure graphite adhesive.

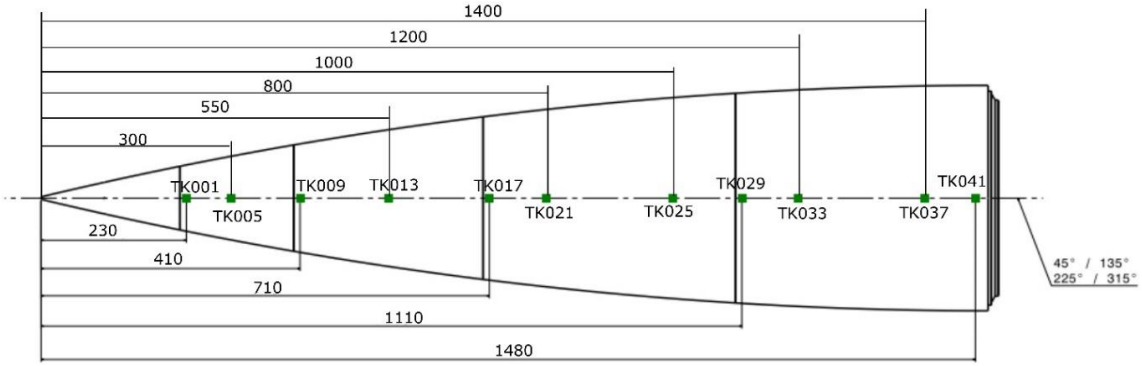

Fig. 13. Axial thermocouple positions on the STORT forebody with name tags for the 45° line. TCs were positioned on four lines from the stagnation point downstream separated by 90° angles.

In the nose tip there were thermocouples positioned at various depths according to Fig. 14. Those were type S elements. The most forward element TS001V was placed at 34 mm distance from the actual stagnation point on the centerline at a radial distance of 10 mm from the surface, next to it, also at an axial distance of 34 mm and at 5 mm radial distance from the surface was TS002V. Further downstream, at 150 mm axial distance from the tip and 3 mm and 9 mm radial distance from the surface, repsectively, were elements TS004V and TS003V. Unfortunately, TS001V was damaged during final assembly and could not be replaced for the flight, so TS002V was the most forward measurement point.

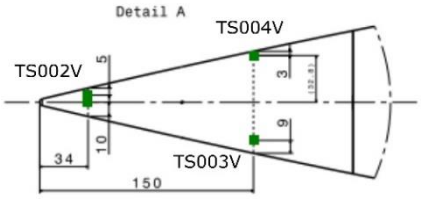

Fig. 14. Thermocouple positions in the STORT nose tip.

In Fig. 15 the measured temperatures in the nose tip from the thermocouples shown in Fig. 14 are presented along with numericl simulations carried out via the simplified approach described above. The numerical simulations were done using the hot wall heat flux, derived as described, and giving this as a thermal load on the external surface of a 3D model in a finite element model of the forebody. The prediction of the thermal loads is quite well matched.

The temperatures in general follow the flight profile and increase during the acceleration phases of the launcher when the velocity increases. There are distinct temperature plateaus during the coast phases after first stage burn and second stage burn when the heat load is not increasing further. During the acceleration of the third stage and the following flight phase at high Mach number, the temperatures continuosly increase. Towards the end of the flight, a pronounced increase at a time of roughly 200 s is visible. This effect can be seen in all of the other temperature measurements at the different segments. The maximum temperature at the x=34 mm position was at 1111 °C (no mistake).

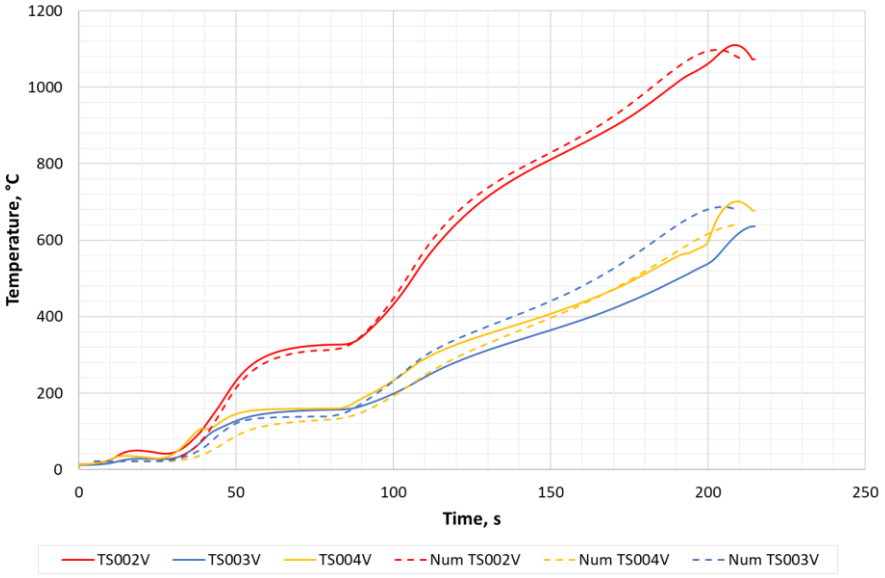

Fig. 15. Measured temperatures in the CMC nose tip.

Another example ist presented for the measurements done in the segment A. Thermocouples were located at the position of x=230 mm just after the forward edge of the segment, directly after the interface to the solid nose tip. The second position of thermocouples was at x=300 mm in the middle of the segment. At each of these two positions, four thermocouples were placed around the circumference, spaced by 90° angles, starting at the 45° line.

On segment A it can be noted that the measurements at one x position are grouped together at similar values. Little differences can be explained by local variations in the placement depth. The temperature curves in general also reflect the flight profile with the two increases due to the launcher acceleration and then the flight at high mach number.

It is interesting to see that the forward position at x=230 mm shows lower temperatures in general. This is due to the fact, that segment a is in physical contact to the solid nose tip component, which acts as a heat sink in its rear part. This becomes especially obvious during the ascent phase after the second stage burn, when there is a temperature plateau developing between 50 and 90 s during the coast phase. Then, the nose temperature at x=150 mm is only 140-160 °C during the plateau time between 50 and 100 s, whereas in segment A the temperature plateau is around 200 °C for the x=230 mm position, and around 350 °C for the x=300 mm position.

In the case of segment A, the numerical prediction matches the measured data quite well for the first part of the flight, with the stage one and two accelerations and the following coast phase. At higher speeds the prediction is overestimating the flight loads.

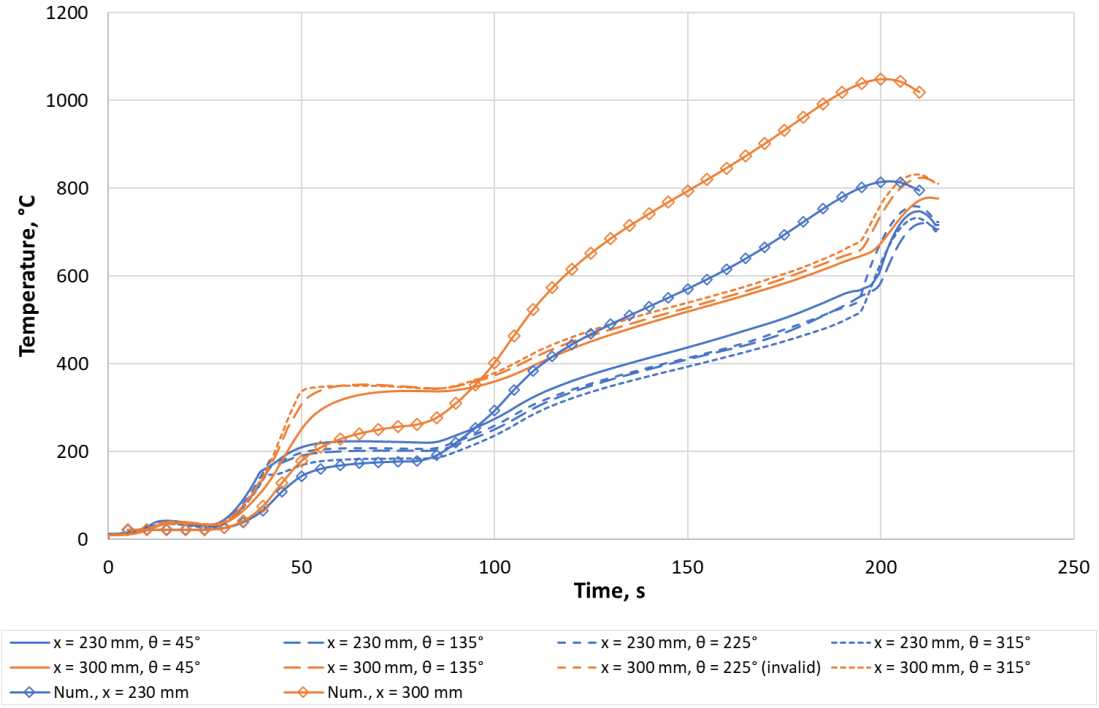

6. Conclusion

The flight of the experimental STORT vehicle was successful in being also the first time that a three-stage sounding rocket system was designed and flown by DLR-MORABA. In particular, the suppressed trajectory at low altitude with the apogee of 38 km was significant because a relatively constant high Mach number around 8 could be maintained for roughly one minute and speeds over Mach 7 for two minutes. Thus, it was possible to collect experimental data over an extended period of time in a demanding aerothermodynamic environment.

It could be shown that a hypersonic flight vehicle could be designed, of which the forebody surface is fully made from CMC structures, to cope with the high heat loads that were expected during the extended flight time at high Mach number. That was essential, because in contrast to propelled vehicle concepts using liquid fuels, where the fuel can act as a heat sink for cooling of structures, STORT did not have this option.

The CMC structures were axisymmetric, thin-walled shell structures to avoid as much as possible flow perturbations. They had to be designed as hot structures due to the extended flight time, which resulted in a high temperature of the complete shell structure. Consequently, the problem of thermal expansion

mismatch between hot shells and cold metallic structure had to be treated. To this end, the so-called double-l connection was implemented, consisting of two l-shaped brackets, one from CMC, the other from Inconel, to balance expansion and bear the mechanical loads. The design analysis proved the viability of the system and it performed well during the pre-flight environmental tests (vibration) and during flight.

The forebody of the vehicle was equipped with a large number of sensors, including thermocouples, heat flux gauges and pressure sensors. The detailed evaluation of the flight data is ongoing. The measured peak temperature in the nose tip was 1111°C, though it has to be mentioned, this position is 34 mm behind the actual stagnation surface on the tip with regard to x position. For the segments A-D the peak temperatures were 778°C, 822°C, 721° and 621°C respectively. The temperatures seem not to be too high at first glance but this has to be seen in perspective. When the measured temperature is compared to the prediction for the position, the difference is small, so it can be assumed that also the tip temperature itself was roughly as predicted at 2200°C. Moreover, even though the flight time was relatively long in comparison to previous hypersonic flight experiments, it has to be noted that the conditions were by no way steady-state yet. There was still significant increase in the temperatures almost everywhere on the vehicle with the exception of a few positions on the canards. This means that in steady-state conditions the temperatures would indeed be still higher.

This is a strong point for considering yet longer flight times at such conditions to finally achieve a situation which is corresponding to steady-state flight. This would require different launcher combinations. A big step towards longer flight duration a such high speeds is the recent qualification for operational use of the Red Kite motor stage which was successfully demonstrated at the end of 2023. To conclude, the presented work is a strong argument for the validity of hypersonic flight research on sounding rockets. The ratio between cost and achieved results is very favourable, as well as the relatively short cycles between flights so that fast gains can be achieved in the technology

Acknowledgments

The support of the workshop and technical staff at the Institute is greatly acknowledged which was of great help to produce and assemble the hardware in time for the flight. The authors wish to thank especially Felix Vogel from the CMC department and Frank Entenmann from Space System Integration for their support.

References

1. Weihs, H., Longo, J., Turner, J.: The Sharp Edge Flight Experiment SHEFEX II, a Mission Overview and Status. 15th AIAA International Space Planes and Hypersonic Systems and Technologies Conference. https://doi.org/10.2514/6.2008-2542.
2. Bauer, W. et al.: DLR Reusability Flight Experiment ReFEx. Acta Astronautica, 168 (2019), pp. 57-68. https://doi.org/10.1016/j.actaastro.2019.11.034.
3. Guédron, S., Ishimoto, S., Dumont, E.: CALLISTO: a Cooperation for an In-Flight Demonstration of Reusability. 70th International Astronautical Congress (IAC), 21-25 October 2019, Washington DC, USA.
4. Gülhan, A., Hargarten, D., Zurkaulen, M., Klingenberg, F., Siebe, F., Willems, S., Di Martino, G., Reimer, T.: Selected Results of the Hypersonic Flight Experiment STORT. Acta Astronautica, Volume 211, October 2023, Pages 333-343, https://doi.org/10.1016/j.actaastro.2023.06.034
5. Kochendorfer,R., Lutzenburger, N., Weihs, H.: Joining Techniques for Fibre Ceramic Structures. *Advanced Composites Letters*, 13 (1) (2004). https://doi.org.10.1177/096369350401300106
6. Van Driest, E.R.: The Problem of Aerodynamic Heating. Aeronaut. Eng. Review, Vol. 15 No. 10, 1956.
7. Mangler, W.: Boundary Layers at Bodies of Revolution in Symmetric Flow. AVA Report 45/A/17 (1945).